Alexandria Engineering Journal (2023) 67, 183–192

HOSTED BY

Alexandria University

Alexandria Engineering Journal

www.elsevier.com/locate/aej
www.sciencedirect.com

ORIGINAL ARTICLE

Brownian and thermophoresis diffusion effects on magnetohydrodynamic Reiner–Philippoff nanofluid flow past a shrinking sheet

Iskandar Waini [a,*], Khairum Bin Hamzah [a], Najiyah Safwa Khashi'ie [a], Nurul Amira Zainal [a], Abdul Rahman Mohd Kasim [b], Anuar Ishak [c], Ioan Pop [d]

[a] *Fakulti Teknologi Kejuruteraan Mekanikal dan Pembuatan, Universiti Teknikal Malaysia Melaka, Hang Tuah Jaya, 76100 Durian Tunggal, Melaka, Malaysia*
[b] *Centre for Mathematical Sciences, Universiti Malaysia Pahang, Lebuhraya Persiaran Tun Khalil Yaakob, 26300 Gambang Pahang, Malaysia*
[c] *Department of Mathematical Sciences, Faculty of Science and Technology, Universiti Kebangsaan Malaysia, 43600 UKM, Bangi, Selangor, Malaysia*
[d] *Department of Mathematics, Babeş-Bolyai University, 400084 Cluj-Napoca, Romania*

Received 25 July 2022; revised 11 December 2022; accepted 24 December 2022
Available online 30 December 2022

KEYWORDS

Reiner–Philippoff fluid;
Nanofluid;
Magnetohydrodynamic;
Thermal radiation;
Brownian and thermophoresis;
Shrinking sheet

Abstract The aim of this paper is to highlight the output of the investigation on the MHD and radiative flow and thermal characteristics of a non-Newtonian Reiner–Philippoff nanofluid with Brownian and thermophoresis diffusion effects. The model studied is embedded in the Buongiorno theory. This unique model is designed to observe both shear thickening and shear thinning properties on that particular fluid with embedded Brownian and thermophoresis diffusion implications. The proposed model consists of continuity, momentum, energy, and concentration equations constructed using the theoretical assumptions and are reduced to a set of ordinary differential equations (ODEs) before solving it using the bvp4c function in MATLAB software. Two solutions are observed, and their physical significance is justified using the temporal stability analysis. From the standpoint of the Reiner–Philippoff fluid parameter, the skin friction coefficient as well as the heat and mass transfer rates are at maximum for the shear-thickening fluid followed by the Newtonian and shear-thinning fluids. The thermophoresis parameter is noticed to decline the heat and mass transfer rate whereas the Brownian motion parameter boosts the mass transfer rate but decreases the heat transfer rate.

* Corresponding author.
E-mail address: iskandarwaini@utem.edu.my (I. Waini).

Peer review under responsibility of Faculty of Engineering, Alexandria University.

https://doi.org/10.1016/j.aej.2022.12.056
1110-0168 © 2022 THE AUTHORS. Published by Elsevier BV on behalf of Faculty of Engineering, Alexandria University.

1. Introduction

Nowadays, the study of nanofluid flow have received much attention from researchers due to its significance in controlling the flow behaviour, as well as the heat and the mass transfer rate in industrial processes. It is important to note that Buongiorno [1] studied the convective transport in nanofluids intending to understand the improvements in heat transfer that were seen during convective circumstances. He downplayed the importance of suspension, particle rotation, dispersion, and turbulence as important factors in enhancing the heat transfer. Buongiorno [1] put forth a brand-new model that is based on the relative velocities of nanoparticles and the base fluids. He concluded that in the absence of turbulent effects, Brownian diffusion and thermophoresis predominate. Based on these two effects, he came up with conservation equations. This discovery was then become the main reference for many researchers who intended to consider the combination of this nanofluid model with various non-Newtonian fluids. To name a few, Saleem et al. [2] and Zokri et al. [3,4] analysed the Jeffrey nanofluid, Waqas et al. [5] and Mahat et al. [6] examined the viscoelastic nanofluid, Shah et al. [7] with Casson nanofluid, and Tlili et al. [8] studied the Maxwell nanofluid flows.

Industrial and technological applications demand effective working fluid in determining the optimum production. Conventionally, pure water (Newtonian) as a cooling agent is used in many processes but the use of the non-Newtonian type of fluid becoming more relevant due to its effectiveness and applicability. There are many types of non-Newtonian fluids available that present a special feature in their properties. Different from the Newtonian type fluid whose strain is in line with stress tensor, the non-Newtonian type is classified by the behavior of either shear-thinning which present pseudo-plasticity, or shear thickening describing the dilatant. The shear-thickening fluid indicates the growth in viscosity proportional to the shear rate, whereas the shear-thinning displays the Newtonian fluid's behavior in extreme values of shear rate. Several fluid models that convey the shear thickening and thinning behaviors have been mentioned in Deshpande et al. [9] including the model of Reiner–Philippoff, Sisko, Powell–Eyring, Carreau–Yasuda as well as Carreau viscosity. Among the models under the non-Newtonian group, the Reiner–Philippoff model is more interesting to research since its exhibits the behaviour of Newtonian fluid at zero or large value of shear stress and behave as non-Newtonian behaviour on other value. Owing to its big significance in engineering applications, the investigation of the Reiner-Philippoff model obtained attention from many researchers where the investigation cover the analysis which the flow moving over different geometries as well as the different effect on the flow field, see Refs. [10–20]. Moreover, other interesting works on the nanofluid flow incorporated with Reiner–Philippoff fluid model in the thin film were considered by Ullah et al. [21], while Ahmad [22] and Li et al. [23] considered the stretching surface.

Embedding thermal radiation to the flow offer more challenges and significant contribution since its presence affected the heat transfer rate. We can find worth application of thermal radiation in the field of solar technology, aeronautic industry, and also spacecraft activities. The thermal radiation was pioneered by Rosseland [24] and the ideas have been widely extended by Ghosh and Mukhopadhyay [25], Yashkun et al. [26], Agbaje et al. [27], and Muhammad et al. [28] in the study of fluid flow covering the non-Newtonian and Newtonian categorized fluid with and without nanoparticles.

The effect of magnetic field or normally written as magnetohydrodynamics (MHD) is among the popular effect considered in fluid flow investigation due to its ability to upshot the fluid characteristics. The presence of MHD launches the drag Lorentz force which can delay the separation of boundary layer. The analysis on the presence of MHD was emphasized in a report by Rashidi et al. [29] where the MHD was applied in energy generators and nuclear propulsion space vehicles. Besides that, Sheikholeslami et al. [30] as well as Hussain et al. [31] conducted the research on MHD flow under free convection mode. On the other hand, Haq et al. [32] studied the MHD flow by embedding the nanoparticles. Other papers on MHD flow were reported by Khan et al. [33,34], Srinivasulu and Goud [35], Khashi'ie et al. [36,37], Zhang et al. [38], and Saranya and Al-Mdallal [39]. Additionally, the study on convective heat transfer in MHD hybrid nanofluid flow over different geometries has been reported by Ashwinkumar et al. [40,41]. Meanwhile, the MHD and heat source effects on parabolic flow over three different non-Newtonian fluids were examined by Samrat et al. [42].

As a novelty, the study of the Reiner–Philippoff fluid model incorporated with nanofluid is limited and offers some gaps to be fulfilled. Hence, this study is aimed to extend the exploration of the special characteristics of the Reiner–Philippoff fluid embedding the Brownian and thermophoresis diffusion with MHD circumstances and radiative heat transfer. The validation procedures are performed by direct comparison with the established models in the limiting case where the models are identical. The inputs of the present computation establish the dual similarity solutions and thus the stability analysis procedures are carried out to determine which solutions are stable. The results of this present investigation can give insight into the study of complex fluid which is normally found in many manufacturing processing and also industrial applications.

2. Mathematical formulation

The steady-two-dimensional boundary layer flow of a Reiner–Philippoff nanofluid past a shrinking surface is considered under the assumption that the external pressure on the plate is in the x-direction and contains nanoparticles in the base fluids. The flow configuration is displayed in Fig. 1. Here, $u_w(x) = ax^{1/3}$ represents the surface velocity with$a > 0$. The

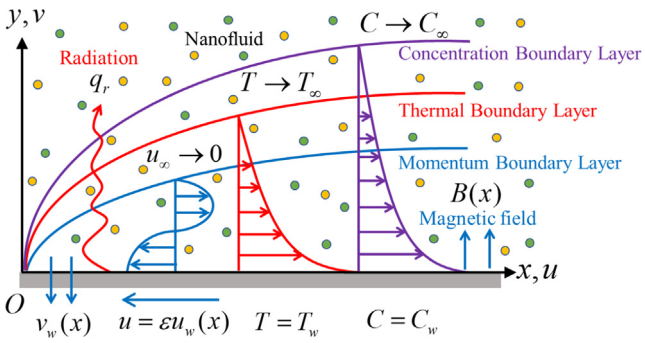

Fig. 1 Flow configuration.

magnetic field $B(x) = B_0 x^{-1/3}$ where B_0 is constant magnetic strength [16]. In addition, Brownian and thermophoresis diffusion (D_B and D_T) effects are employed [21,22]. The radiative heat flux is also considered with $q_r = -(4\sigma^*/3k^*)(\partial T^4/\partial y)$ and $T^4 \cong 4T_\infty^3 T - 3T_\infty^4$ [24]. Here, k^* and σ^* signify the mean absorption and the Stefan-Boltzmann constants, respectively. The model that represents the present problem was first undergoing the boundary layer approximations.

Therefore, the governing boundary layer equations are [21,22]:

$$\frac{\partial u}{\partial x} + \frac{\partial v}{\partial y} = 0 \tag{1}$$

$$\frac{\partial u}{\partial y} = \frac{\tau}{\mu_\infty + \frac{\mu_0 - \mu_\infty}{1+\left(\frac{\tau}{\tau_s}\right)^2}} \tag{2}$$

$$u\frac{\partial u}{\partial x} + v\frac{\partial u}{\partial y} = \frac{1}{\rho}\frac{\partial \tau}{\partial y} - \frac{\sigma}{\rho}B^2 u \tag{3}$$

$$u\frac{\partial T}{\partial x} + v\frac{\partial T}{\partial y} = \left(\frac{k}{\rho C_p} + \frac{16\sigma^* T_\infty^3}{3(\rho C_p)k^*}\right)\frac{\partial^2 T}{\partial y^2} + \delta\left(D_B\frac{\partial C}{\partial y}\frac{\partial T}{\partial y} + \frac{D_T}{T_\infty}\left(\frac{\partial T}{\partial y}\right)^2\right) \tag{4}$$

$$u\frac{\partial C}{\partial x} + v\frac{\partial C}{\partial y} = D_B\frac{\partial^2 C}{\partial y^2} + \frac{D_T}{T_\infty}\frac{\partial^2 T}{\partial y^2} \tag{5}$$

subjected to the following boundary condition as once considered by [21,22,43,44]:

$$\begin{aligned} &u = \varepsilon u_w(x),\ \ v = v_w(x),\ \ T = T_w,\ \ C = C_w \ \text{ at } \ y = 0;\\ &u \to 0,\ \ T \to T_\infty,\ \ C \to C_\infty \ \text{ as } \ y \to \infty \end{aligned} \tag{6}$$

with the reference shear stressτ_s, the shear stressτ, the zero-shear dynamic viscosityμ_0, and the limiting dynamic viscosity μ_∞ [20]. Moreover, ρC_p is the heat capacity, δ is the effective heat capacity ratio, σ is the electric conductivity, ρ is the fluid density, and k is the thermal conductivity. It is assumed that at the shrinking surface, the temperature T and the nanoparticle volume fraction C take constant values T_w and C_w whereas the ambient values of temperature T_∞ and the nanoparticle fraction C_∞ are attained as y tends to infinity.

Consider the similarity variables [21,22,43,44]:

$$\begin{aligned} &\psi = \sqrt{av}x^{2/3}f(\eta),\ \ \tau = \rho\sqrt{a^3 v}g(\eta),\\ &\theta(\eta) = \frac{T - T_\infty}{T_w - T_\infty},\ \ \chi(\eta) = \frac{C - C_\infty}{C_w - C_\infty},\ \ \eta = \frac{y}{x^{1/3}}\sqrt{\frac{a}{v}} \end{aligned} \tag{7}$$

with the stream functionψ. Here:

$$\begin{aligned} u &= \frac{\partial \psi}{\partial y} = ax^{1/3}f'(\eta),\quad v = -\frac{\partial \psi}{\partial x}\\ &= -\sqrt{av}x^{-1/3}\left(\frac{2}{3}f(\eta) - \frac{1}{3}\eta f'(\eta)\right) \end{aligned} \tag{8}$$

and:

$$v_w(x) = -\frac{2}{3}\sqrt{av}x^{-1/3}S \tag{9}$$

with $v = \mu_\infty/\rho$ is the fluid kinematic viscosity. Meanwhile, constant mass flux parameter is denoted by$f(0) = S$. Here, $S = 0$ and $S > 0$ denote the impermeable and the suction cases. Then, one obtains:

$$g = f'\left(\frac{\lambda\gamma^2 + g^2}{\gamma^2 + g^2}\right) \tag{10}$$

$$g\prime + \frac{2}{3}ff'' - \frac{1}{3}f'^2 - Mf' = 0 \tag{11}$$

$$\frac{1}{\Pr}\left(1 + \frac{4}{3}R\right)\theta'' + \frac{2}{3}f\theta' + Nb\chi'\theta' + Nt\theta'^2 = 0 \tag{12}$$

$$\chi'' + Scf\chi' + \frac{Nt}{Nb}\theta'' = 0 \tag{13}$$

subject to:

$$\begin{aligned} &f(0) = S,\ \ f'(0) = \varepsilon,\ \ \theta(0) = 1,\ \ \chi(0) = 1;\\ &f'(\eta) \to 0,\ \ \theta(\eta) \to 0,\ \ \chi(\eta) \to 0 \ \text{ as } \ \eta \to \infty \end{aligned} \tag{14}$$

with $\varepsilon = 0$ (static sheet), $\varepsilon > 0$ (stretching sheet) and $\varepsilon < 0$ (shrinking sheet). Moreover, the Prandtl numberPr, the Schmidt numberSc, the magnetic parameter$M$, the Reiner–Philippoff fluidλ, the thermal radiation$R$, the Bingham numberγ, the Brownian motion parameterNb, and the thermophoresis parameter Nt are defined as:

$$\begin{aligned} &\Pr = \tfrac{\mu C_p}{k},\ \ Sc = \tfrac{v}{D_B},\ \ M = \tfrac{\sigma}{\rho a}B_0^2,\ \ \lambda = \tfrac{\mu_0}{\mu_\infty},\ \ R = \tfrac{4\sigma^* T_\infty^3}{kk^*},\\ &\gamma = \tfrac{\tau_s}{\rho\sqrt{a^3 v}},\ \ Nb = \tfrac{\delta D_B\ (C_w - C_\infty)}{v},\ \ Nt = \tfrac{\delta D_T\ (T_w - T_\infty)}{v\ T_\infty} \end{aligned} \tag{15}$$

The physical quantities are given as:

$$Sh_x = \frac{xq_m}{D_B(C_w - C_\infty)},\quad Nu_x = \frac{xq_w}{k(T_w - T_\infty)},\quad C_f = \frac{\tau_w}{\rho\, u_w^2} \tag{16}$$

where q_m (surface mass flux), q_w (surface heat flux) and τ_w (value of τ on $y = 0$) are:

$$\begin{aligned} &q_m = -D_B\left(\frac{\partial C}{\partial y}\right)_{y=0},\quad q_w = -k\left(\frac{\partial T}{\partial y}\right)_{y=0} + (q_r)_{y=0},\\ &\tau_w = \rho\sqrt{a^3 v}(g(\eta))_{y=0} \end{aligned} \tag{17}$$

which then yield

$$\begin{aligned} &\mathrm{Re}_x^{-1/2}Sh_x = -\chi'(0),\\ &\mathrm{Re}_x^{-1/2}Nu_x = -\left(1 + \frac{4}{3}R\right)\theta'(0),\quad \mathrm{Re}_x^{1/2}C_f = g(0) \end{aligned} \tag{18}$$

with $\mathrm{Re}_x^{-1/2}Sh_x$ and $Nu_x\mathrm{Re}_x^{-1/2}$ denote the local Sherwood number and the local Nusselt number, respectively, and $C_f\mathrm{Re}_x^{1/2}$ indicates the skin friction coefficient where $\mathrm{Re}_x = u_w(x)x/v$ signifies the local Reynolds number.

3. Stability analysis

The execution of the stability analysis is done in this section [45,46]. Thus, the new variables are introduced [20]:

$$\begin{aligned} &\psi = \sqrt{av}x^{2/3}f(\eta,\Gamma),\ \ \tau = \rho\sqrt{a^3 v}g(\eta,\Gamma),\\ &\theta(\eta,\Gamma) = \tfrac{T - T_\infty}{T_w - T_\infty},\ \ \chi(\eta,\tau) = \tfrac{C - C_\infty}{C_w - C_\infty},\\ &\eta = \tfrac{y}{x^{1/3}}\sqrt{\tfrac{a}{v}},\ \ \Gamma = \tfrac{a}{x^{2/3}}t \end{aligned} \tag{19}$$

with the dimensionless time variable,Γ. Here:

$$u = ax^{1/3}\frac{\partial f}{\partial \eta}(\eta,\Gamma),$$
$$v = -\sqrt{av}x^{-1/3}\left(\tfrac{2}{3}f(\eta,\Gamma) - \tfrac{1}{3}\eta\frac{\partial f}{\partial \eta}(\eta,\Gamma) - \tfrac{2}{3}\Gamma\frac{\partial f}{\partial \Gamma}(\eta,\Gamma)\right) \tag{20}$$

Employing the unsteady flow, one obtains:

$$\frac{\partial u}{\partial t} + u\frac{\partial u}{\partial x} + v\frac{\partial u}{\partial y} = \frac{1}{\rho}\frac{\partial \tau}{\partial y} - \frac{\sigma}{\rho}B^2 u \tag{21}$$

$$\frac{\partial T}{\partial t} + u\frac{\partial T}{\partial x} + v\frac{\partial T}{\partial y} = \left(\frac{k}{\rho C_p} + \frac{16\sigma^* T_\infty^3}{3(\rho C_p)k^*}\right)\frac{\partial^2 T}{\partial y^2} + \delta\left(D_B\frac{\partial C}{\partial y}\frac{\partial T}{\partial y} + \frac{D_T}{T_\infty}\left(\frac{\partial T}{\partial y}\right)^2\right) \tag{22}$$

$$\frac{\partial C}{\partial t} + u\frac{\partial C}{\partial x} + v\frac{\partial C}{\partial y} = D_B\frac{\partial^2 C}{\partial y^2} + \frac{D_T}{T_\infty}\frac{\partial^2 T}{\partial y^2} \tag{23}$$

while Eqs. (1) and (2) remain unchanged. Thus:

$$g = \frac{\partial^2 f}{\partial \eta^2}\left(\frac{\lambda\gamma^2 + g^2}{\gamma^2 + g^2}\right) \tag{24}$$

$$\frac{\partial g}{\partial \eta} + \frac{2}{3}f\frac{\partial^2 f}{\partial \eta^2} - \frac{1}{3}\left(\frac{\partial f}{\partial \eta}\right)^2 - M\frac{\partial f}{\partial \eta} - \frac{\partial^2 f}{\partial \eta \partial \Gamma} - \frac{2}{3}\Gamma\left(\frac{\partial f}{\partial \Gamma}\frac{\partial^2 f}{\partial \eta^2} - \frac{\partial f}{\partial \eta}\frac{\partial^2 f}{\partial \eta \partial \Gamma}\right) = 0 \tag{25}$$

$$\tfrac{1}{\Pr}\left(1 + \tfrac{4}{3}R\right)\tfrac{\partial^2 \theta}{\partial \eta^2} + \tfrac{2}{3}f\tfrac{\partial \theta}{\partial \eta} + Nb\tfrac{\partial \chi}{\partial \eta}\tfrac{\partial \theta}{\partial \eta} + Nt\left(\tfrac{\partial \theta}{\partial \eta}\right)^2 - \tfrac{\partial \theta}{\partial \Gamma} - \tfrac{2}{3}\Gamma\left(\tfrac{\partial f}{\partial \Gamma}\tfrac{\partial \theta}{\partial \eta} - \tfrac{\partial f}{\partial \eta}\tfrac{\partial \theta}{\partial \Gamma}\right) = 0 \tag{26}$$

$$\frac{\partial^2 \chi}{\partial \eta^2} + \frac{2}{3}Scf\frac{\partial \chi}{\partial \eta} + \frac{Nt}{Nb}\frac{\partial^2 \theta}{\partial \eta^2} - Sc\frac{\partial \chi}{\partial \Gamma} - \frac{2}{3}Sc\Gamma\left(\frac{\partial f}{\partial \Gamma}\frac{\partial \chi}{\partial \eta} - \frac{\partial f}{\partial \eta}\frac{\partial \chi}{\partial \Gamma}\right) = 0 \tag{27}$$

subject to:

$$f(0,\Gamma) - \tfrac{2}{3}\Gamma\tfrac{\partial f}{\partial \Gamma}(0,\Gamma) = S,\ \ \tfrac{\partial f}{\partial \eta}(0,\Gamma) = \varepsilon,\ \ \theta(0,\Gamma) = 1,$$
$$\chi(0,\Gamma) = 1;\ \ \tfrac{\partial f}{\partial \eta}(\eta,\Gamma) \to 0,\ \ \theta(\eta,\Gamma) \to 0, \tag{28}$$
$$\chi(\eta,\Gamma) \to 0 \text{ as } \eta \to \infty$$

Then, the perturbation functions are introduced [46]:

$$f(\eta,\Gamma) = f_0(\eta) + e^{-\alpha\Gamma}F(\eta,\Gamma),\ \ g(\eta,\Gamma) = g_0(\eta) + e^{-\alpha\Gamma}G(\eta,\Gamma),$$
$$\theta(\eta,\Gamma) = \theta_0(\eta) + e^{-\alpha\Gamma}H(\eta,\Gamma),\ \ \chi(\eta,\Gamma) = \chi_0(\eta) + e^{-\alpha\Gamma}J(\eta,\Gamma) \tag{29}$$

where $F(\eta,\Gamma)$, $G(\eta,\Gamma)$, $H(\eta,\Gamma)$, and $J(\eta,\Gamma)$ are arbitrary functions and α denotes the eigenvalue. By setting $\Gamma = 0$, then $F(\eta,\Gamma) = F_0(\eta)$, $G(\eta,\Gamma) = G_0(\eta)$, $H(\eta,\Gamma) = H_0(\eta)$, and $J(\eta,\Gamma) = J_0(\eta)$. Therefore:

$$G_0 = F_0''\left(\frac{\lambda\gamma^2 + g_0^2}{\gamma^2 - 2f_0'' g_0 + 3g_0^2}\right) \tag{30}$$

$$G_0' + \frac{2}{3}\left(f_0 F_0'' + f_0'' F_0\right) - \frac{2}{3}f_0' F_0 - MF_0' + \alpha F_0' = 0 \tag{31}$$

$$\frac{1}{\Pr}\left(1 + \frac{4}{3}R\right)H_0'' + \frac{2}{3}\left(f_0 H_0' + \theta_0' F_0\right) + Nb\left(\chi_0' H_0' + \theta_0' J_0'\right) + 2Nt\theta_0' H_0' + \alpha H_0 = 0 \tag{32}$$

$$J_0'' + \frac{2}{3}Sc\left(f_0 J_0' + \chi_0' F_0\right) + \frac{Nt}{Nb}H_0'' + Sc\alpha J_0 = 0 \tag{33}$$

subject to:

$$F_0(0) = 0,\ \ F_0'(0) = 0,\ \ H_0(0) = 0,\ \ J_0(0) = 0;$$
$$F_0'(\eta) \to 0,\ \ H_0(\eta) \to 0,\ \ J_0(\eta) \to 0 \text{ as } \eta \to \infty \tag{34}$$

Here, to obtain α from Eqs. (30)-(33), $F_0'(\eta) \to 0$ as $\eta \to \infty$ in Eq. (34) is replaced by $F''(0) = 1$ as employed in [47–49].

4. Results and discussion

Equations (10)-(13) with the corresponding initial and boundary conditions (14) have been solved numerically using the bvp4c scheme in the MATLAB platform [50]. The influences of the non-dimensional governing parameters on the skin friction coefficient $\mathrm{Re}_x^{1/2}C_f$, local Nusselt number $\mathrm{Re}_x^{-1/2}Nu_x$, local Sherwood number $\mathrm{Re}_x^{-1/2}Sh_x$, velocity profiles $f'(\eta)$, temperature profiles $\theta(\eta)$, and concentration profiles $\chi(\eta)$ have been established by assigning some numerical values to the nondimensional parameters.

In order to check the accuracy and validity of the present results, Table 1 displays the values of $g(0)$ produced in this study and those reported by Sajid et al. [17]. Further validations for the values of $-\theta'(0)$ are shown in Table 2 where the comparison is made between the present results with those obtained by Waini et al. [51], Cortell [52], and Ferdows et al. [53]. The generated results shown in Tables 1 and 2 revealed a noteworthy agreement with previous findings hence confirmed the precision of mathematical formulation in the current work. In addition, the newly computed results for the values of $\mathrm{Re}_x^{1/2}C_f$, $\mathrm{Re}_x^{-1/2}Nu_x$, and $\mathrm{Re}_x^{-1/2}Sh_x$ under various physical parameters are given in Table 3.

The influence of Nb and Nt on the temperature and concentration profiles are presented in Figs. 2-5. The upsurges of Nb thickens the thermal boundary layer but the concentration boundary layer decreases (see Figs. 2 and 4). These observations imply that the rising of Nb tends to increase the intensity of the mass transfer rate but decreases the heat transfer rate. Meanwhile, the impact of Nt is to increase both the thermal and the concentration boundary layers (see Figs. 3 and 5) which lead to the decrement of the heat and the mass transfer

Table 1 Values of $g(0)$ for γ and λ when $S = M = 0$ and $\varepsilon = 1$.

γ	λ	Present Result	Sajid et al. [17]
0.1	0.1	−0.660275	−0.660273
0.5		−0.380604	−0.380604
1		−0.246415	−0.246415
0.1	0.3	−0.664498	−0.664497
	0.5	−0.668486	−0.668484
	0.7	−0.672277	−0.672282
	1	−0.677648	

Table 2 Values of $-\theta'(0)$ for R and S when$\varepsilon = \lambda = \gamma = 1, M = Nb = Nt = 0$, and$\mathrm{Pr} = 2$.

R	S	Waini et al. [51]	Cortell [52]	Ferdows et al. [53]	Present Result
0	0.5	1.230792	1.2307661	1.230952	1.230792
	0	0.764357	0.7643554	0.764374	0.764357
	−0.5	0.399100	0.3989462	0.398951	0.399100
1	0.5	0.632200	0.6322154	0.632199	0.632200
	0	0.443323	0.4430879	0.443323	0.443323
	−0.5	0.287485	0.2873762	0.287483	0.287484

Table 3 Values of$\mathrm{Re}_x^{1/2} C_f$,$\mathrm{Re}_x^{-1/2} Nu_x$, and $\mathrm{Re}_x^{-1/2} Sh_x$ for various values of physical parameters when$\varepsilon = -1, S = 2.4, \gamma = 0.1$,$\mathrm{Pr} = 7$, and$Sc = 5$.

λ	M	R	Nb	Nt	$\mathrm{Re}_x^{1/2} C_f$	$\mathrm{Re}_x^{-1/2} Nu_x$	$\mathrm{Re}_x^{-1/2} Sh_x$
0.5	0.01	5	0.1	0.1	1.172320	8.115112	6.308563
1					1.153161	8.054998	6.304251
1.5					1.127876	7.984054	6.299091
1.5	0				1.102980	7.946854	6.296085
	0.015				1.138984	7.999908	6.300388
	0.02				1.149432	8.014435	6.301586
	0.01	3			1.127876	8.073701	5.683904
		3.5			1.127876	8.066222	5.886497
		4			1.127876	8.045975	6.050276
		5	0.2		1.127876	7.372610	6.991041
			0.3		1.127876	6.805216	7.219763
			0.5		1.127876	5.791366	7.399564
			0.1	0.2	1.127876	7.690126	5.079019
				0.3	1.127876	7.410676	3.936049
				0.5	1.127876	6.892089	1.860863

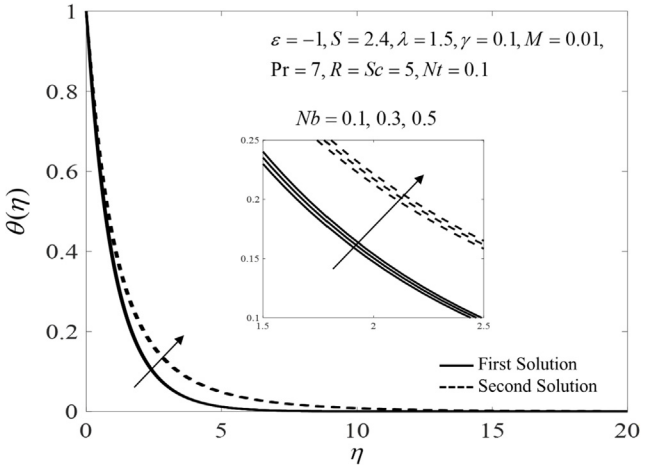

Fig. 2 Temperature profiles $\theta(\eta)$ for various values of the Brownian motion parameterNb.

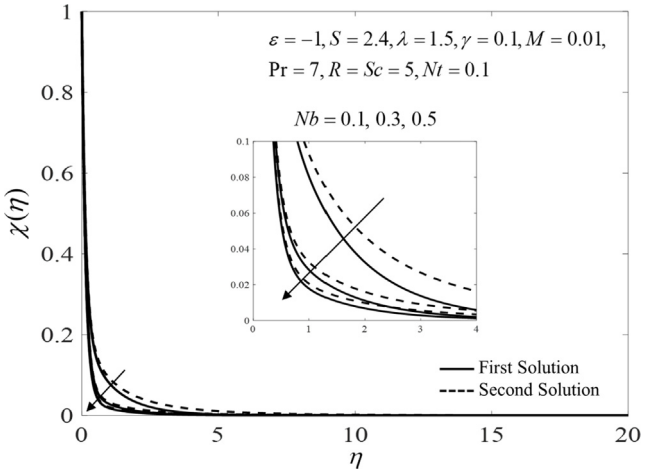

Fig. 3 Concentration profiles $\chi(\eta)$ for various values of the Brownian motion parameterNb.

rates. Additionally, Figs. 6 and 7 are provided to get a clear insight of Nb and Nt effects on the heat and the mass transfer rates. From the physical point of view, the Brownian motion causes a collision between the fluid particles. Therefore, the rising of Nb causes an increment in the fluid temperature due to the kinetic energy produced by the suspended nanoparticles and consequently generates the thermophoretic force. Thus, the fluid is driven to flow away from the surface due to the

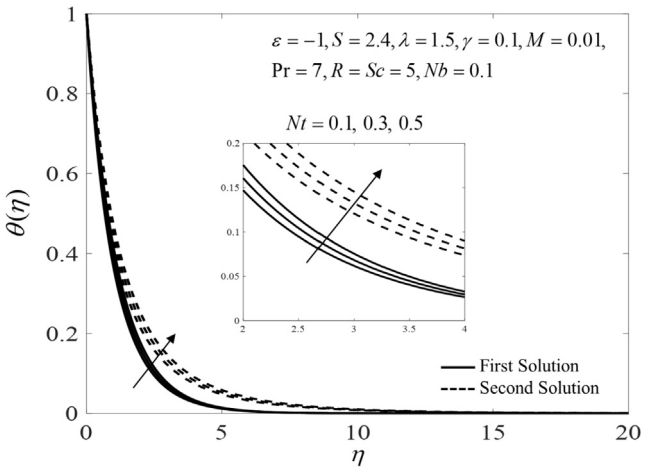

Fig. 4 Temperature profiles $\theta(\eta)$ for various values of the thermophoresis parameterNt.

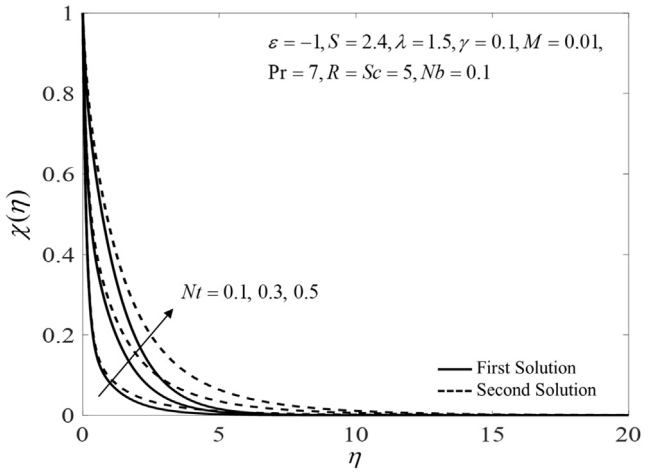

Fig. 5 Concentration profiles $\chi(\eta)$ for various values of the thermophoresis parameterNt.

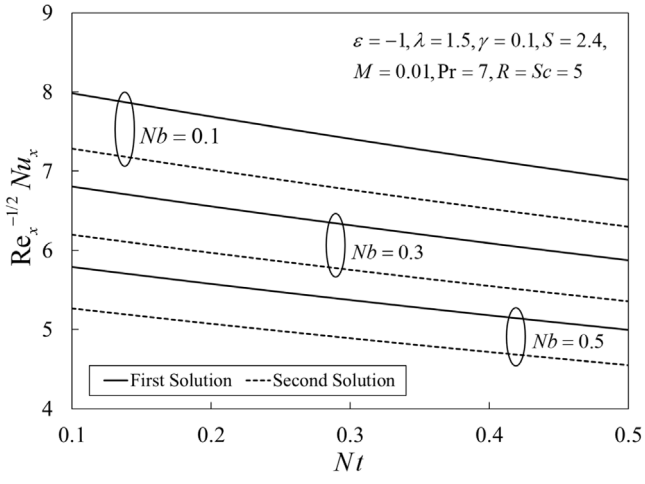

Fig. 6 Local Nusselt number $\mathrm{Re}_x^{-1/2} Nu_x$ against Nt for various values ofNb.

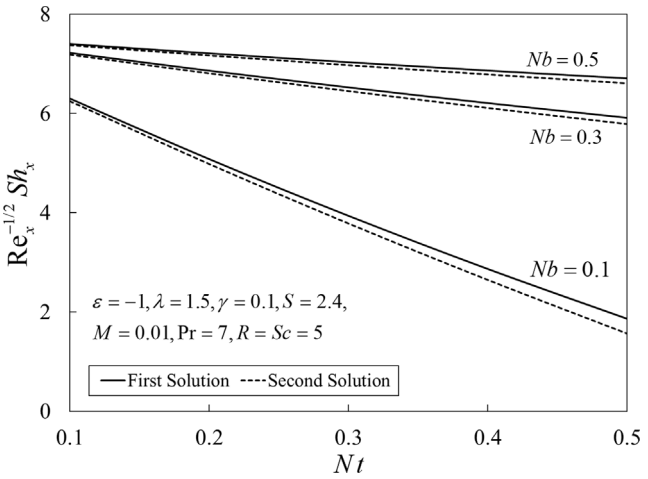

Fig. 7 Local Sherwood number $\mathrm{Re}_x^{-1/2} Sh_x$ against Nt for various values ofNb.

force's intensity. As a result, higher values of Nt result in an increase in the fluid concentration, as well as raises the fluid temperature.

The impact of the thermal radiation parameter R on the local Nusselt number$\mathrm{Re}_x^{-1/2} Nu_x$, and the local Sherwood number $\mathrm{Re}_x^{-1/2} Sh_x$ when$\varepsilon=-1$, $S=2.4$, $\gamma=0.1$, $M=0.01$, $\Pr=7$, $Sc=5$, and $Nb=Nt=0.1$ are deliberated in Figs. 8 and 9, respectively. It is found that the distribution of $\mathrm{Re}_x^{-1/2} Nu_x$ reduces with the increasing of$R$. Physically, the occurrence of thermal radiation results in an increase of the radiative heat flux over the functional flow. Henceforth, the inclusion in R leads to an increase in the boundary layer thickness, thus the temperature distribution in the flow region rises as R intensifies. In contrast, the values of $\mathrm{Re}_x^{-1/2} Sh_x$ are intensified with larger values of$R$. Since higher temperature occurs for larger$R$, therefore, it leads to the reduction of the fluid concentration near the surface by thinning its boundary layer. Consequently, the concentration gradient increases which lead to the enhancement of the mass transfer rate. Besides, it is seen from Figs. 8 and 9 that the critical value of S_c is unchanged for

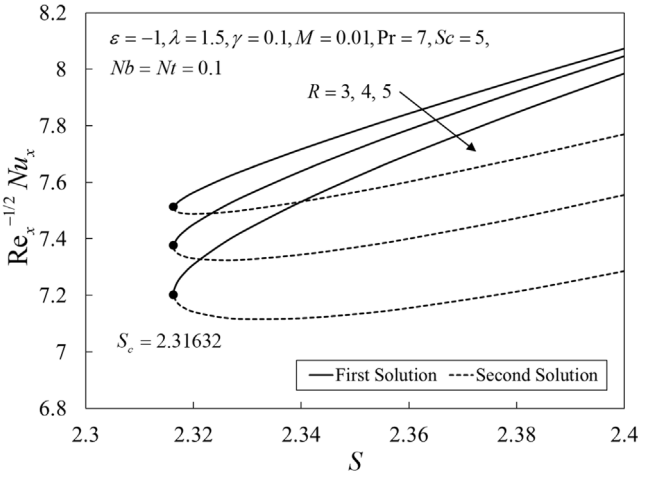

Fig. 8 Local Nusselt number $\mathrm{Re}_x^{-1/2} Nu_x$ against mass flux parameter S for various R.

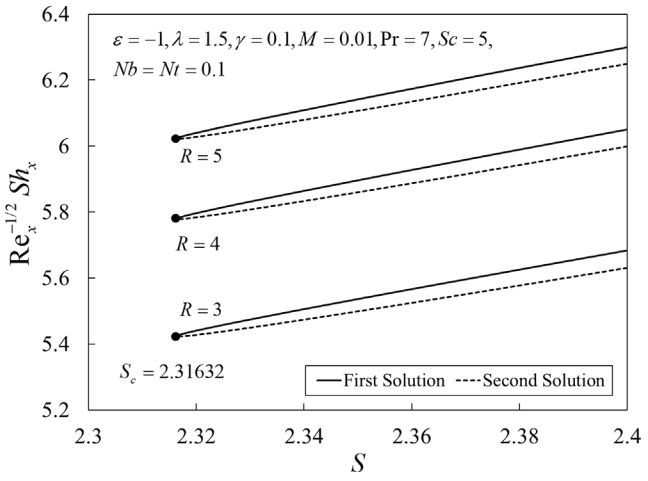

Fig. 9 Local Sherwood number $\mathrm{Re}_x^{-1/2} Sh_x$ against mass flux parameter S for various R.

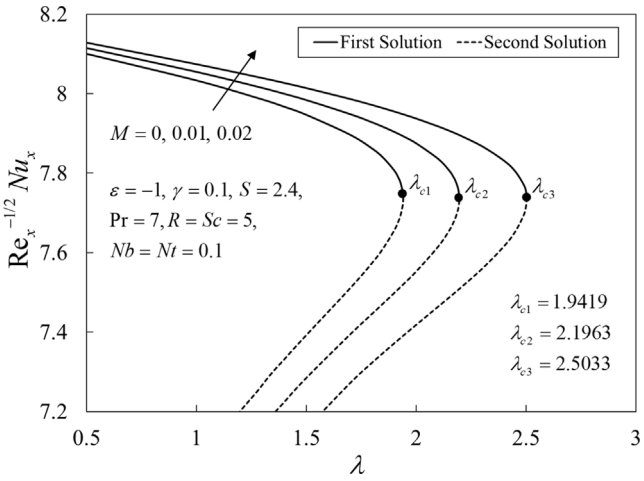

Fig. 11 Local Nusselt number $\mathrm{Re}_x^{-1/2} Nu_x$ against λ for various M.

different values of R, where $S_c = 2.31632$ for each value of R considered.

Meanwhile, Figs. 10-12 show the variations of $\mathrm{Re}_x^{1/2} C_f$,$\mathrm{Re}_x^{-1/2} Nu_x$, and $\mathrm{Re}_x^{-1/2} Sh_x$ against λ for different values of M. The critical values are $\lambda_{c1} = 1.9419$ $(M = 0)$, $\lambda_{c2} = 2.1963$ $(M = 0.01)$, and $\lambda_{c3} = 2.5033$ $(M = 0.02)$ which prove that the domain of the solution is also dependent on λ. Besides, all these physical quantities enlarge with the increase of M. From physical point of view, magnetic field generates Lorentz force, which is a resistive force that emerges when a transverse magnetic field is applied and engaged with an electrically conducting fluid. The strength of the Lorentz force increases as the strength of the applied magnetic field intensifies, acting in the opposite direction of fluid movement within the boundary layer. Furthermore, this parameter develops the concentration and thermal properties which lead to boosting the rate of the mass and heat transfer processes.

The variations of $\mathrm{Re}_x^{1/2} C_f$,$\mathrm{Re}_x^{-1/2} Nu_x$, and $\mathrm{Re}_x^{-1/2} Sh_x$ for different values of S and λ are shown in Figs. 13-15. The critical values are $S_{c1} = 2.17656$ $(\lambda = 0.5)$,$S_{c2} = 2.24990$ $(\lambda = 1)$, and $S_{c3} = 2.31632$ $(\lambda = 1.5)$. Physically, the Reiner-Philippoff fluid

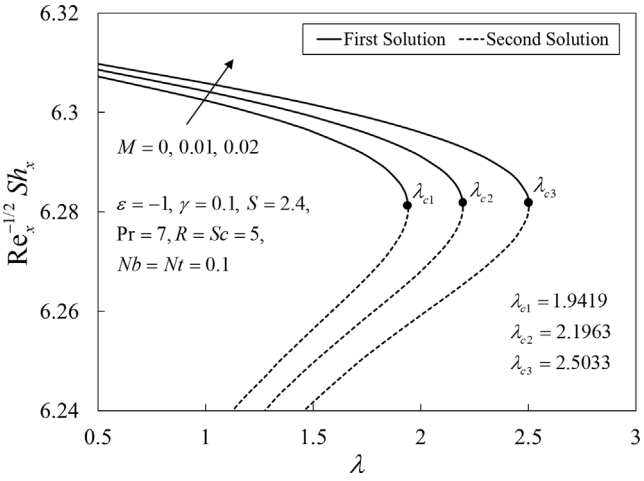

Fig. 12 Local Sherwood number $\mathrm{Re}_x^{-1/2} Sh_x$ against λ for various M.

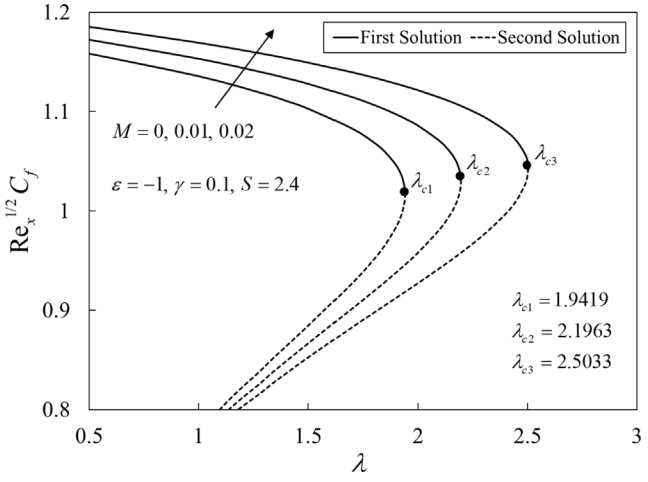

Fig. 10 Skin friction coefficient $\mathrm{Re}_x^{1/2} C_f$ against λ for various M.

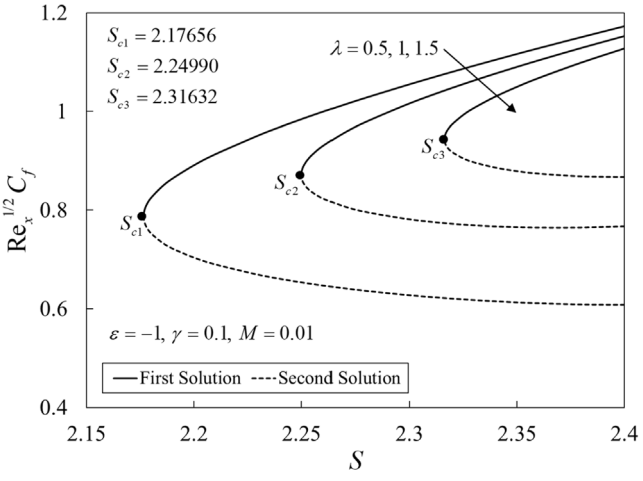

Fig. 13 Skin friction coefficient $\mathrm{Re}_x^{1/2} C_f$ against S for variousλ.

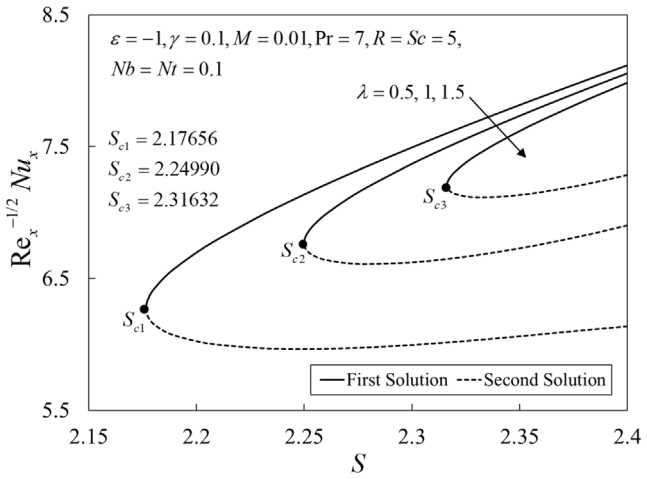

Fig. 14 Local Nusselt number $\mathrm{Re}_x^{-1/2} Nu_x$ against S for variousλ.

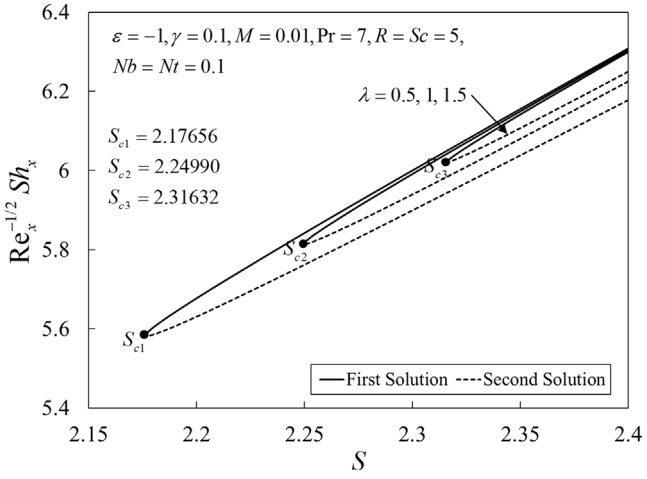

Fig. 15 Local Sherwood number $\mathrm{Re}_x^{-1/2} Sh_x$ against S for variousλ.

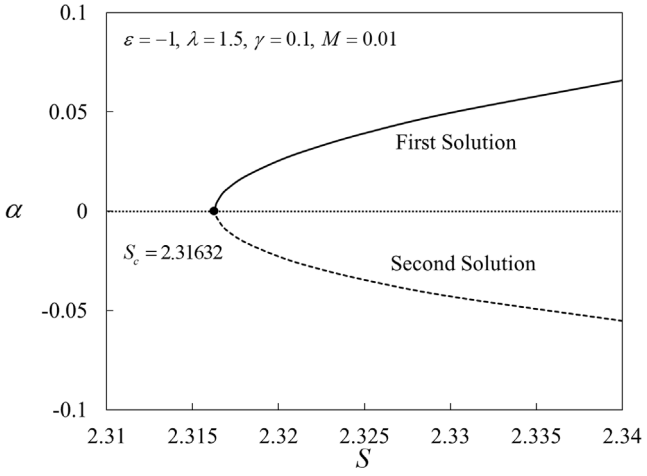

Fig. 16 Smallest eigenvalues α against mass flux parameter$S$.

parameter represents the zero shear viscosity ratio to the upper Newton limiting viscosity. From Fig. 13, it shows that increasing the values of λ leads to a decrease in the skin friction coefficient. This is due to the fact that increasing λ values cause a reduction in viscosity, allowing the fluid to move around more freely and thus lowering the coefficient of the skin friction. Since the energy and concentration equations are coupled with the momentum equation, thus, it directly affects the magnitudes of$\mathrm{Re}_x^{-1/2} Nu_x$, and $\mathrm{Re}_x^{-1/2} Sh_x$ as shown in Figs. 14 and 15.

Fig. 16 presents the variations of the smallest eigenvalues α against S with the negative eigenvalue designating the second solution while the positive eigenvalue indicating the first solution. Based on the perturbation functions (29), the unsteady solutions converge to the steady-state solutions for $\alpha > 0$ as time evolves,$\Gamma \to \infty$. On the other hand, the solutions diverge for $\alpha < 0$ as$\Gamma \to \infty$. This leads to the conclusion that the first solution is stable and reliable over time, but the second solution behaves in the opposite way.

5. Conclusion

An analysis of magnetohydrodynamic and radiative heat and mass transfer of Reiner–Philippoff nanofluid flow over a nonlinearly shrinking sheet with Brownian and thermophoresis diffusion effects was considered mathematically. The decrement of the friction factor, the local Nusselt number, and the Sherwood number are observed with the rise of the Reiner–Philippoff fluid parameter. In contrast, these physical quantities increase for larger values of the magnetic parameter due to higher Lorentz's force. Furthermore, the increase of the Brownian motion parameter Nb tends to intensify the mass transfer rate but decreases the heat transfer rate. Meanwhile, the rising of the thermophoresis parameter Nt lead to the decrement of the heat and the mass transfer rates. However, increasing the radiation parameter leads to a reduction in thermal and mass progress. From the computed smallest eigenvalues in the stability analysis, it is found that only the first solution is physically stable in the long run.

Declaration of Competing Interest

The authors declare that they have no known competing financial interests or personal relationships that could have appeared to influence the work reported in this paper.

Acknowledgments

The authors gratefully acknowledge Universiti Teknikal Malaysia Melaka (JURNAL/2019/FTKMP/Q00042), Universiti Kebangsaan Malaysia, and Universiti Malaysia Pahang for the financial supports.

References

[1] J. Buongiorno, Convective transport in nanofluids, J. Heat Transfer 128 (2006) 240–250, https://doi.org/10.1115/1.2150834.
[2] S. Saleem, H. Rafiq, A. Al-Qahtani, M.A. El-Aziz, M.Y. Malik, I.L. Animasaun, Magneto Jeffrey nanofluid bioconvection over a rotating vertical cone due to gyrotactic microorganism, Math. Probl. Eng. 2019 (2019) 3478037, https://doi.org/10.1155/2019/3478037.

[3] S.M. Zokri, M.Z. Salleh, A.R. Mohd Kasim, N.S. Arifin, Lower stagnation point flow of convectively heated horizontal circular cylinder in Jeffrey nanofluid with suction/injection, Journal of Advanced Research in Fluid Mechanics and Thermal Sciences 76 (2020) 135–144. https://doi.org/10.37934/arfmts.76.1.135.
[4] S.M. Zokri, N.S. Arifin, A.R.M. Kasim, M.Z. Salleh, Flow of Jeffrey fluid over a horizontal circular cylinder with suspended nanoparticles and viscous dissipation effect: Buongiorno model, CFD Letters 12 (2020) 1–13. https://doi.org/10.37934/cfdl.12.11.113.
[5] M. Waqas, M.M. Gulzar, A.S. Dogonchi, M.A. Javed, W.A. Khan, Darcy-Forchheimer stratified flow of viscoelastic nanofluid subjected to convective conditions, Appl. Nanosci. 9 (2019) 2031–2037, https://doi.org/10.1007/s13204-019-01144-9.
[6] R. Mahat, N.A. Rawi, A.R.M. Kasim, S. Shafie, Heat generation effect on mixed convection flow of viscoelastic nanofluid: Convective boundary condition solution, Malaysian Journal of Fundamental and Applied Sciences 16 (2020) 166–175. https://doi.org/10.11113/mjfas.v16n2.1367.
[7] Z. Shah, P. Kumam, W. Deebani, Radiative MHD Casson nanofluid flow with activation energy and chemical reaction over past nonlinearly stretching surface through Entropy generation, Sci. Rep. 10 (2020) 4402, https://doi.org/10.1038/s41598-020-61125-9.
[8] I. Tlili, S. Naseer, M. Ramzan, S. Kadry, Y. Nam, Effects of chemical species and nonlinear thermal radiation with 3D Maxwell nanofluid flow with double stratification-an analytical solution, Entropy 22 (2020) 453, https://doi.org/10.3390/E22040453.
[9] A.P. Deshpande, J.M. Krishnan, P.B.S. Kumar, Rheology of Complex Fluids, Springer, New York (2010), https://doi.org/10.1007/978-1-4419-6494-6.
[10] J.N. Kapur, R.C. Gupta, Two dimensional flow of Reiner-Philippoff fluids in the inlet length of a straight channel, Applied Scientific Research 14 (1964) 13–24.
[11] O.N. Cavatorta, R.D. Tonini, Dimensionless velocity profiles and parameter maps for non-Newtonian fluids, International Communications in Heat and Mass Transfer 14 (1987) 359–369.
[12] A.G. Hansen, T.Y. Na, Similarity solutions of laminar, incompressible boundary layer equations of non-newtonian fluids, Journal of Basic Engineering 90 (1968) 71–74, https://doi.org/10.1115/1.3605067.
[13] T.Y. Na, Boundary layer flow of Reiner-Philippoff fluids, Int. J. Non-Linear Mech. 29 (1994) 871–877, https://doi.org/10.1016/0020-7462(94)90059-0.
[14] A. Ahmad, M. Qasim, S. Ahmed, Flow of Reiner-Philippoff fluid over a stretching sheet with variable thickness, Journal of the Brazilian Society of Mechanical Sciences and Engineering 39 (2017) 4469–4473, https://doi.org/10.1007/s40430-017-0840-7.
[15] M.G. Reddy, S. Rani, K.G. Kumar, A.H. Seikh, M. Rahimi-Gorji, E.S.M. Sherif, Transverse magnetic flow over a Reiner-Philippoff nanofluid by considering solar radiation, Modern Physics Letters B 33 (2019) 1950449, https://doi.org/10.1142/S0217984919504499.
[16] K.G. Kumar, M.G. Reddy, M.V.V.N.L. Sudharani, S.A. Shehzad, A.J. Chamkha, Cattaneo-Christov heat diffusion phenomenon in Reiner-Philippoff fluid through a transverse magnetic field, Physica A: Statistical Mechanics and Its Applications 541 (2020), https://doi.org/10.1016/j.physa.2019.123330 123330.
[17] T. Sajid, M. Sagheer, S. Hussain, Impact of temperature-dependent heat source/sink and variable species diffusivity on radiative Reiner-Philippoff fluid, Math. Probl. Eng. 2020 (2020) 9701860, https://doi.org/10.1155/2020/9701860.
[18] I. Waini, A.R.M. Kasim, N.S. Khashi'ie, N.A. Zainal, A. Ishak, I. Pop, Insight into stability analysis on modified magnetic field of radiative non-Newtonian Reiner – Philippoff fluid model, Journal of Advanced Research in Applied Mechanics 8 (2022) 745–753. https://doi.org/10.22055/JACM.2022.38820.3287.
[19] N.S. Khashi'ie, I. Waini, A.R.M. Kasim, N.A. Zainal, A. Ishak, I. Pop, Magnetohydrodynamic and viscous dissipation effects on radiative heat transfer of non-Newtonian fluid flow past a nonlinearly shrinking sheet: Reiner–Philippoff model, Alexandria Engineering Journal 61 (2022) 7605–7617. https://doi.org/10.1016/j.aej.2022.01.014.
[20] K.S. Yam, S.D. Harris, D.B. Ingham, I. Pop, Boundary-layer flow of Reiner-Philippoff fluids past a stretching wedge, Int. J. Non Linear Mech. 44 (2009) 1056–1062, https://doi.org/10.1016/j.ijnonlinmec.2009.08.006.
[21] A. Ullah, E.O. Alzahrani, Z. Shah, M. Ayaz, S. Islam, Nanofluids thin film flow of Reiner-Philippoff fluid over an unstable stretching surface with Brownian motion and thermophoresis effects, Coatings 9 (2019) 21, https://doi.org/10.3390/coatings9010021.
[22] A. Ahmad, Flow of ReinerPhilippoff based nano-fluid past a stretching sheet, J. Mol. Liq. 219 (2016) 643–646, https://doi.org/10.1016/j.molliq.2016.03.068.
[23] Y.X. Li, H. Waqas, K. Al-Khaled, S. Hussain, S.U. Khan, T.C. Sun, M.I. Khan, M.Y. Malik, I. Tlili, Study of radiative Reiner-Philippoff nanofluid model with gyrotactic microorganisms and activation energy: A Cattaneo-Christov double diffusion (CCDD) model analysis, Chinese Journal of Physics 73 (2021) 569–580, https://doi.org/10.1016/j.cjph.2021.08.003.
[24] S. Rosseland, Astrophysik und atom-theoretische Grundlagen, Springer-Verlag, Berlin, 1931.
[25] S. Ghosh, S. Mukhopadhyay, Unsteady MHD three-dimensional flow of nanofluid over a stretching surface with zero nanoparticles flux and thermal radiation, Waves in Random and Complex Media. (2022) Published online. https://doi.org/10.1080/17455030.2021.1965671.
[26] U. Yashkun, K. Zaimi, N.A. Abu Bakar, A. Ishak, I. Pop, MHD hybrid nanofluid flow over a permeable stretching/shrinking sheet with thermal radiation effect, Int. J. Numer. Methods Heat Fluid Flow 31 (2021) 1014–1031, https://doi.org/10.1108/HFF-02-2020-0083.
[27] T.M. Agbaje, S. Mondal, S.S. Motsa, P. Sibanda, A numerical study of unsteady non-Newtonian Powell-Eyring nanofluid flow over a shrinking sheet with heat generation and thermal radiation, Alexandria Engineering Journal 56 (2017) 81–91, https://doi.org/10.1016/j.aej.2016.09.006.
[28] K. Muhammad, T. Hayat, A. Alsaedi, Heat transfer analysis in slip flow of hybrid nanomaterial (Ethylene Glycol + Ag + CuO) via thermal radiation and Newtonian heating, Waves in Random and Complex Media. (2022) Published online. https://doi.org/10.1080/17455030.2021.1950947.
[29] M.M. Rashidi, S. Abelman, N.F. Mehr, Entropy generation in steady MHD flow due to a rotating porous disk in a nanofluid, Int. J. Heat Mass Transf. 62 (2013) 515–525, https://doi.org/10.1016/j.ijheatmasstransfer.2013.03.004.
[30] M. Sheikholeslami, M. Gorji-Bandpy, D.D. Ganji, MHD free convection in an eccentric semi-annulus filled with nanofluid, J. Taiwan Inst. Chem. Eng. 45 (2014) 1204–1216, https://doi.org/10.1016/j.jtice.2014.03.010.
[31] S.M. Hussain, J. Jain, G.S. Seth, M.M. Rashidi, Free convective heat transfer with Hall effects, heat absorption and chemical reaction over an accelerated moving plate in a rotating system, J. Magn. Magn. Mater. 422 (2017) 112–123, https://doi.org/10.1016/j.jmmm.2016.08.081.
[32] R.U. Haq, I. Rashid, Z.H. Khan, Effects of aligned magnetic field and CNTs in two different base fluids over a moving slip surface, J. Mol. Liq. 234 (2017) 682–688, https://doi.org/10.1016/j.molliq.2017.08.084.
[33] U. Khan, A. Zaib, I. Khan, K.S. Nisar, Activation energy on MHD flow of titanium alloy (Ti6Al4V) nanoparticle along with a cross flow and streamwise direction with binary chemical

reaction and non-linear radiation: Dual solutions, Journal of Materials Research and Technology 9 (2020) 188–199, https://doi.org/10.1016/j.jmrt.2019.10.044.
[34] U. Khan, A. Zaib, I. Khan, D. Baleanu, E.S.M. Sherif, Comparative investigation on MHD nonlinear radiative flow through a moving thin needle comprising two hybridized AA7075 and AA7072 alloys nanomaterials through binary chemical reaction with activation energy, Journal of Materials Research and Technology 9 (2020) 3817–3828, https://doi.org/10.1016/j.jmrt.2020.02.008.
[35] T. Srinivasulu, B.S. Goud, Effect of inclined magnetic field on flow, heat and mass transfer of Williamson nanofluid over a stretching sheet, Case Studies in Thermal Engineering 23 (2021), https://doi.org/10.1016/j.csite.2020.100819 100819.
[36] N.S. Khashi'ie, N.M. Arifin, M.M. Rashidi, E.H. Hafidzuddin, N. Wahi, Magnetohydrodynamics (MHD) stagnation point flow past a shrinking/stretching surface with double stratification effect in a porous medium, J. Therm. Anal. Calorim. 139 (2020) 3635–3648. https://doi.org/10.1007/s10973-019-08713-8.
[37] N.S. Khashi'ie, N.M. Arifin, I. Pop, Magnetohydrodynamics (MHD) boundary layer flow of hybrid nanofluid over a moving plate with Joule heating, Alexandria Engineering Journal 61 (2022) 1938–1945. https://doi.org/10.1016/j.aej.2021.07.032.
[38] X.H. Zhang, A. Abidi, A.E.S. Ahmed, M.R. Khan, M.A. El-Shorbagy, M. Shutaywi, A. Issakhov, A.M. Galal, MHD stagnation point flow of nanofluid over a curved stretching/shrinking surface subject to the influence of Joule heating and convective condition, Case Studies in Thermal Engineering 26 (2021), https://doi.org/10.1016/j.csite.2021.101184 101184.
[39] S. Saranya, Q.M. Al-Mdallal, Non-Newtonian ferrofluid flow over an unsteady contracting cylinder under the influence of aligned magnetic field, Case Studies in Thermal Engineering 21 (2020), https://doi.org/10.1016/j.csite.2020.100679 100679.
[40] G.P. Ashwinkumar, S.P. Samrat, N. Sandeep, Convective heat transfer in MHD hybrid nanofluid flow over two different geometries, International Communications in Heat and Mass Transfer 127 (2021), https://doi.org/10.1016/j.icheatmasstransfer.2021.105563 105563.
[41] G.P. Ashwinkumar, M. Girinath Reddy, N. Sandeep, Convective heat transfer in MHD Cu-TiO2-H2O cross nanofluid flow over three diverse surfaces, Proceedings of the Institution of Mechanical Engineers, Part E: Journal of Process Mechanical Engineering 236 (2022) 1800–1807, https://doi.org/10.1177/09544089221076696.
[42] S.P. Samrat, Y.H. Gangadharaiah, G.P. Ashwinkumar, N. Sandeep, Effect of exponential heat source on parabolic flow of three different non-Newtonian fluids, Proceedings of the Institution of Mechanical Engineers, Part E: Journal of Process Mechanical Engineering 236 (2022) 2131–2138, https://doi.org/10.1177/09544089221083468.
[43] A. Pantokratoras, Comment on the paper "MHD slip flow of a dissipative Casson fluid over a moving geometry with heat source/sink: A numerical study, C.S.K. Raju, N. Sandeep, Acta Astronautica 133 (2017) 436–443," Acta Astronaut. 187 (2021) 335–337. https://doi.org/10.1016/j.actaastro.2021.06.041.
[44] P. De, D. Pal, H. Mondal, U.K. Bera, Effect of thermophoresis and Brownian motion on magnetohydrodynamic convective-radiative heat and mass transfer of a nanofluid over a nonlinear stretching sheet, Journal of Nanofluids 6 (2017) 164–172, https://doi.org/10.1166/jon.2017.1290.
[45] J.H. Merkin, On dual solutions occurring in mixed convection in a porous medium, J. Eng. Math. 20 (1986) 171–179, https://doi.org/10.1007/BF00042775.
[46] P.D. Weidman, D.G. Kubitschek, A.M.J. Davis, The effect of transpiration on self-similar boundary layer flow over moving surfaces, Int. J. Eng. Sci. 44 (2006) 730–737, https://doi.org/10.1016/j.ijengsci.2006.04.005.
[47] S.D. Harris, D.B. Ingham, I. Pop, Mixed convection boundary-layer flow near the stagnation point on a vertical surface in a porous medium: Brinkman model with slip, Transp Porous Media. 77 (2009) 267–285, https://doi.org/10.1007/s11242-008-9309-6.
[48] I. Waini, A. Ishak, I. Pop, Hybrid nanofluid flow over a permeable non-isothermal shrinking surface, Mathematics 9 (2021) 538.
[49] I. Waini, A. Ishak, I. Pop, Hybrid nanofluid flow on a shrinking cylinder with prescribed surface heat flux, Int. J. Numer. Methods Heat Fluid Flow 31 (2021) 1987–2004, https://doi.org/10.1108/HFF-07-2020-0470.
[50] L.F. Shampine, I. Gladwell, S. Thompson, Solving ODEs with MATLAB, Cambridge University Press, Cambridge, 2003, https://doi.org/https://doi.org/10.1017/cbo9780511615542.
[51] I. Waini, A. Ishak, I. Pop, Hybrid nanofluid flow and heat transfer over a nonlinear permeable stretching/shrinking surface, Int. J. Numer. Methods Heat Fluid Flow 29 (2019) 3110–3127, https://doi.org/10.1108/HFF-01-2019-0057.
[52] R. Cortell, Heat and fluid flow due to non-linearly stretching surfaces, Appl. Math. Comput. 217 (2011) 7564–7572, https://doi.org/10.1016/j.amc.2011.02.029.
[53] M. Ferdows, M.J. Uddin, A.A. Afify, Scaling group transformation for MHD boundary layer free convective heat and mass transfer flow past a convectively heated nonlinear radiating stretching sheet, Int. J. Heat Mass Transf. 56 (2013) 181–187, https://doi.org/10.1016/j.ijheatmasstransfer.2012.09.020.